A Computational Fluid Dynamic Study on Polymer Heat Exchangers

Mingkan Zhang[1]*, Kashif Nawaz[1]*, Kai Li[1], Tyler Smith[2]

[1]Buildings and Transportation Science Division, Oak Ridge National Laboratory,
Oak Ridge, TN 37830, USA

[2]Manufacturing Science Division, Oak Ridge National Laboratory,
2350 Cherahala Blvd, Knoxville, TN 37932, USA

* Corresponding Author: (M.Z.) Zhangm1@ornl.gov; (K.N.) nawazk@ornl.gov

ABSTRACT

Polymer heat exchangers have been developed for the applications involving weight restrictions or chemical compatibility and fouling issues owing to the low density, anticorrosive properties, and low thermal expansion of polymers. Recently development of additive manufacturing also brings new opportunities to make polymer heat exchangers with desired design that was hard to realize before. However, due to the lower thermal conductivity polymer composite, the overall heat transfer performance is still a challenge in the polymer heat exchanger technology. In present work, a computational fluid dynamic (CFD) model has been developed to study the overall heat transfer performance of additively manufactured polymer heat exchangers. The CFD results offer an insight of fluid flow and temperature distribution in the polymer heat exchangers. This study provides a guidance not only on the polymer material selection but also on the design of polymer heat exchangers. The conclusions will be helpful to design a polymer heat exchanger whose overall heat transfer performance is comparable to a metal heat exchanger.

1. INTRODUCTION

Heat exchangers are essential components for both cooling and heating process. They are widely used in space cooling, air conditioning, refrigeration, energy storages, and chemical plants. Conventionally, metals, e.g., copper and aluminum, are used as the heat exchanger material. However, in some applications, metal materials are suffering from fouling issues due to corrosion, and weight restrictions due to the high density. Polymer heat exchangers have been developed for the applications involving weight restrictions or chemical compatibility and fouling issues owing to the low density, anticorrosive properties, and low thermal expansion of polymers (Wang *et al.*, 2019; Kim and Yoo, 2020). Recent, additive manufacturing techniques have developed rapidly and been implemented in variance fields (Bhargava, Thompson and Malmstadt, 2014). Complex structures can be manufactured by 3D printing with high precision. In addition, additive manufacturing techniques fabricate products without the need of mold or tool, which can save cost and reduce lead time (Ben-Ner and Siemsen, 2017). It provides new opportunities to fabricate 3D complex parts for polymer heat exchangers with desired design that was hard to manufacture before (Ngo *et al.*, 2006; Maloney *et al.*, 2012; Cormier *et al.*, 2013). Integrating additive manufacturing techniques into polymer heat exchangers has a strong potential, especially in producing customized and complex heat exchangers.

However, although a lot of studies have been dedicated to enhancing the thermal conductivity of polymer materials (Guo *et al.*, 2021), the thermal conductivity of polymer heat exchangers is still very low comparing to metal heat exchangers. As a result, overall heat transfer performance is still a challenge in the polymer heat exchanger technology. In present work, a CFD model has been developed to investigate the heat transfer performance of additively manufactured polymer heat exchangers. The CFD model provides an insight of the overall performance of the polymer heat exchanger. Parametric studies are conducted to reveal the key factors influencing the performance. The heat exchanger designs are improved by adding fins to the baseline design. Performance improvement is calculated from the simulation results. The CFD model provides a guidance to the polymer heat exchanger design as well as an assessment of the overall performance of the polymer heat exchanger.

2. SIMULATION DOMAIN

A 3D CFD model was developed using a commercial code Ansys Fluent (Version 17.2) (ANSYS, 2017). Ansys Fluent is installed in a workstation with an Intel Xeon E5-2630 v3 processor and 64 GB memory. The CFD model was based on the 3D printed heat exchanger design. The heat exchanger mainly comprises 103 additively manufactured polymer tubes and two manifolds connecting the ends of the tubes as shown in Figure 1. The manifolds connect to the water supply pipe (diameter of 0.04 m); in the model, the top manifold is the water inlet, and the bottom manifold is the water outlet (the outlet is not shown in Figure 1). The deployment of the tubes is staggered as depicted in Figure 1. The cross-section of a single tube is an ellipse, in which the major axis is 0.017 m long and the minor axis is 0.0075 m long. The tube is 0.305 m long and 1 mm thick. In this work, hot air is blown from one side of the heat exchanger, where it exchanges heat, and leaves from the other side. On the other side of the heat exchanger, cold water is injected from the top manifold (water inlet), passes the tubes, and exhausts from the bottom manifold (water outlet) as shown in Figure 2. To enhance the heat transfer performance of the heat exchanger, extra fins are added between the tubes. Considering the feasibility of additive manufacturing, the fins were designed in a snake shape instead of plate fins being added between tubes. Two types of fins, Snake A and Snake B, were designed as shown in Figure 3. Snake A is the plate fins between tubes with a support between fins to affix the fins to the tubes. Snake B adds an extra vertical plate fin in Snake A. The heat exchanger without fins is the baseline heat exchanger, Snake A is used in Heat Exchanger A, and Snake B is used in Heat Exchanger B.

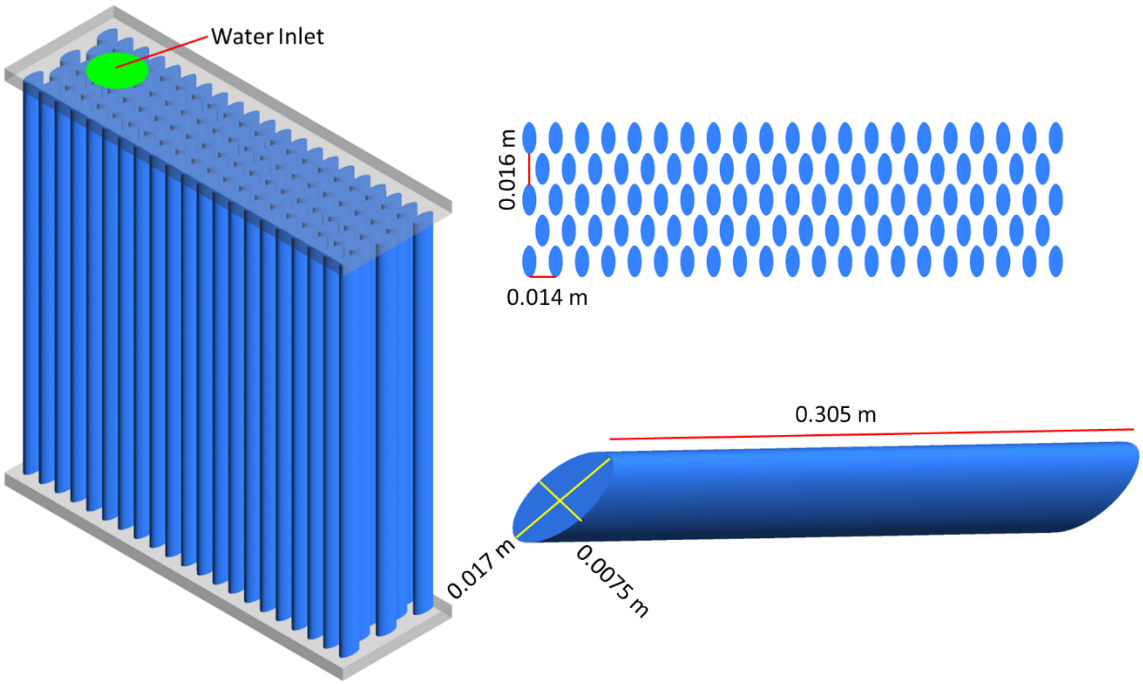

Figure 1: A schematic view of the baseline heat exchanger and tube matrix**.**

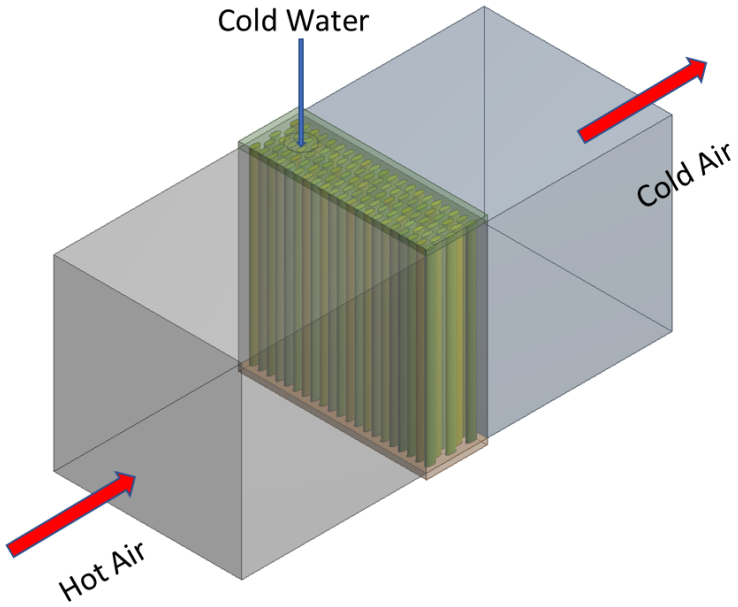

Figure 2: A schematic view of the simulation domain.

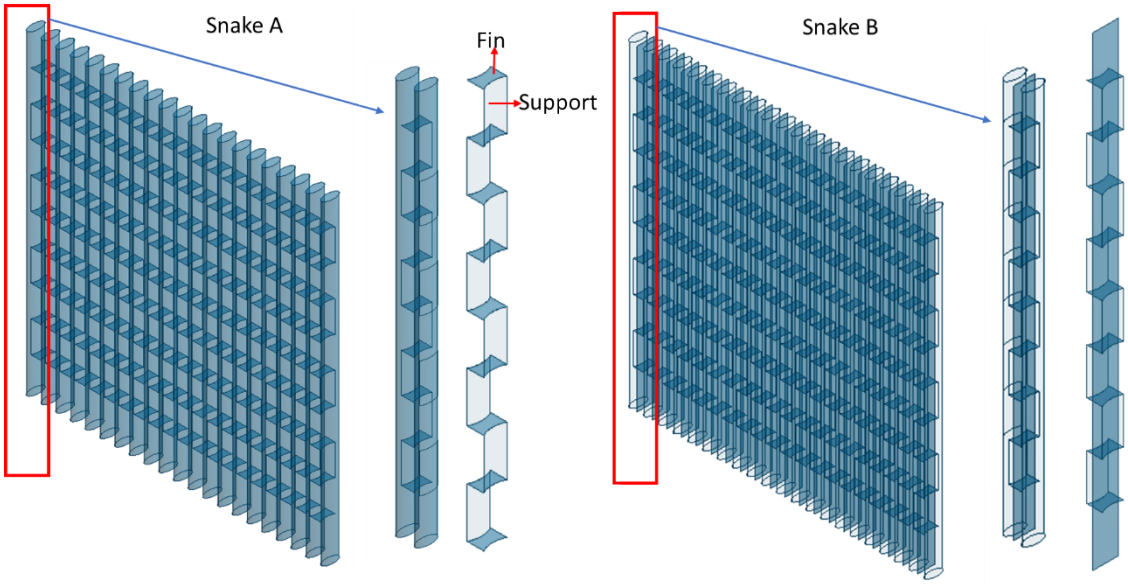

Figure 3: Two types of fins added to the tubes, Snake A and Snake B**.**

3. MATHEMATICAL MODELS

The governing equations considered for the fluid flow and heat transfer include the continuity, momentum, and energy equations. In the present model, two phases of fluids are considered, including air and water. In the model, the continuity and momentum equations are written as

$$\frac{\partial \rho}{\partial t} + \frac{\partial (\rho u_i)}{\partial x_i} = 0 \,, \tag{1}$$

$$\frac{\partial (\rho u_i)}{\partial t} + \frac{\partial (\rho u_i u_j)}{\partial x_j} = -\frac{\partial p}{\partial x_i} + \frac{\partial}{\partial x_j}\left[\mu\left(\frac{\partial u_j}{\partial x_i} + \frac{\partial u_i}{\partial x_j} - \frac{2}{3}\delta_{ij}\frac{\partial u_k}{\partial x_k}\right) - \rho\overline{u_i' u_j'}\right], \tag{2}$$

where u, ρ, p, and μ are fluid velocity vector, density, pressure, and dynamic viscosity, respectively.
Because the fluid flow is turbulent in both tank and heat exchangers, a standard k-ε model was adopted in the model. The Reynolds stress term is

$$-\rho\overline{u_i' u_j'} = \mu_t\left(\frac{\partial u_j}{\partial x_i} + \frac{\partial u_i}{\partial x_j}\right) - \frac{2}{3}\left(\rho k + \mu_t \frac{\partial u_k}{\partial x_k}\right)\delta_{ij} \,, \tag{3}$$

where μ_t is the turbulence dynamic viscosity and calculated by introducing turbulence kinetic energy k and turbulence dissipation rate ε as

$$\mu_t = \rho C_\mu \frac{k^2}{\varepsilon} \,, \tag{4}$$

$$\frac{\partial (\rho k)}{\partial t} + \frac{\partial (\rho k u_i)}{\partial x_i} = \frac{\partial}{\partial x_j}\left[\left(\mu + \frac{\mu_t}{\sigma_k}\right)\frac{\partial k}{\partial x_j}\right] - \rho\overline{u_i' u_j'}\frac{\partial u_j}{\partial x_i} - \rho\varepsilon \,, \tag{5}$$

$$\frac{\partial (\rho \varepsilon)}{\partial t} + \frac{\partial (\rho \varepsilon u_i)}{\partial x_i} = \frac{\partial}{\partial x_j}\left[\left(\mu + \frac{\mu_t}{\sigma_\varepsilon}\right)\frac{\partial \varepsilon}{\partial x_j}\right] - C_{1\varepsilon}\frac{\varepsilon}{k}\left(\rho\overline{u_i' u_j'}\frac{\partial u_j}{\partial x_i}\right) - C_{2\varepsilon}\rho\frac{\varepsilon^2}{k} \,, \tag{6}$$

where the parameters $c_\mu = 0.09$, $c_{\varepsilon 1} = 1.44$, $c_{\varepsilon 2} = 1.92$, $\sigma_k = 1.0$, and $\sigma_\varepsilon = 1.3$ are determined from experimental data (Deylami *et al.*, 2013).
The energy equation is

$$\frac{\partial}{\partial t}(\rho E) + \frac{\partial (\rho E u_i + p u_i)}{\partial x_i} = \nabla \cdot (\lambda_{\text{eff}} \nabla T), \tag{7}$$

where

$$E = h - \frac{p}{\rho} + \frac{v^2}{2}, \tag{8}$$

and

$$\lambda_{\text{eff}} = \lambda + \lambda_t \,. \tag{9}$$

where λ is the thermal conductivity of air, λ_t is the turbulent thermal conductivity. In Eq. (7) and (8), T and h represent the temperature and the enthalpy of the air, which are related with Eq. (10).

$$h = \int_{T_{ref}}^{T} c_p \mathrm{d}T + \frac{p}{\rho} \,. \tag{10}$$

where $T_{\text{ref}} = 298.15$ K and c_{p} is the specific heat of air.
At the air inlet, the air temperature was 45°C. The water temperature at the water inlet was 10°C. The material employed was a polyethylene terephthalate glycol based composite reinforced with 10 wt% pitch fiber and 20 wt% graphite. From lab measurements, the density was 2,161 kg/m^3, the specific heat was 555.3 J/(kg·K), and the thermal conductivity was 1.33 W/(m·K). In the transient simulations, the initial temperatures for both air and water were 26.85°C.

Because the fins are affixed to the tube wall with high thermal conductivity epoxy (5200 silver epoxy), the equivalent thermal conductivity of the tube walls with fin support attached had to be calculated. Figure 4 shows the schematic of the tube wall with fin support attached. The equivalent thermal conductivity of the tube wall with fin support attached in Figure 4 is derived as,

$$\lambda_{eq} = \frac{(L_1 + L_2 + L_3)\lambda_1\lambda_2\lambda_3}{(\lambda_1\lambda_2 L_3 + \lambda_1\lambda_3 L_2 + \lambda_2\lambda_3 L_1)}. \tag{11}$$

The thermal conductivities of the tube, epoxy, and support were $\lambda_1 = 1.33$ W/(m·K), $\lambda_2 = 2.5$ W/(m·K), and $\lambda_3 = 1.33$ W/(m·K), respectively, and the thicknesses of the tube, epoxy, and support were $L_1 = 1$ mm, $L_2 = 0.2$ mm, and $L_3 = 0.5$ mm, respectively. Therefore, the equivalent thermal conductivity was $\lambda_{eq} = 1.4705$ W/(m·K).

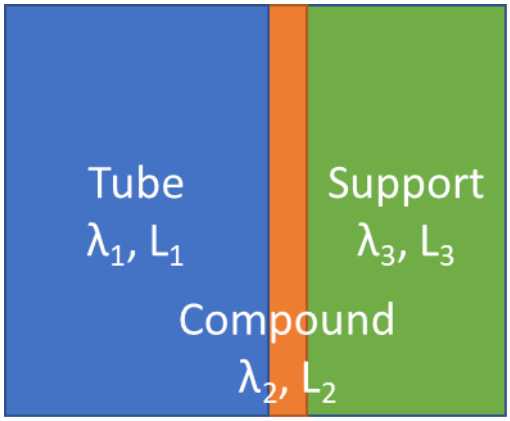

Figure 4: Tube wall with snake support attached.

4. RESULTS AND DISCUSSION

To investigate the performance of the baseline heat exchanger, a matrix of simulations was designed as shown in Table 1, in which the influences of tube thermal conductivity (λ− and λ+), tube wall thickness (Thickness− and Thickness+), water velocity (Water− and Water+), and air velocity (Air− and Air+) were tested by comparing against the reference case of the baseline heat exchanger. Based on the matrix, transient simulations were conducted for all nine cases (the reference case and the others as summarized). Figure 5 depicts the airflow path lines of the reference case, which show that the airflow enters the heat exchanger at 45°C and goes through the heat exchanger with the temperature dropping. Figure 6 plots the air outlet and water outlet temperature changes with time from the different cases. Figure 6 shows that for all the cases, all the outlet temperatures reach a steady state in less than 5 min, indicating that the polymer heat exchanger only needs a relatively short time to reach a steady state, even the tube thermal conductivity is not high. Table 2 lists the outlet temperatures for all cases after 10 min simulations.

Table 1: Simulation matrix of baseline cases

Case	Thermal conductivity (W/(m·K))	Tube wall thickness (mm)	Water velocity (m/s)	Air velocity (m/s)	Air inlet temperature (°C)	Water inlet temperature (°C)
Reference	1.33	1	0.1	0.1214	45	10
λ−	0.4	1	0.1	0.1214	45	10
λ+	8	1	0.1	0.1214	45	10
Thickness−	1.33	0.5	0.1	0.1214	45	10
Thickness+	1.33	2	0.1	0.1214	45	10
Water−	1.33	1	0.05	0.1214	45	10
Water+	1.33	1	0.2	0.1214	45	10
Air−	1.33	1	0.1	0.0607	45	10
Air+	1.33	1	0.1	0.2428	45	10

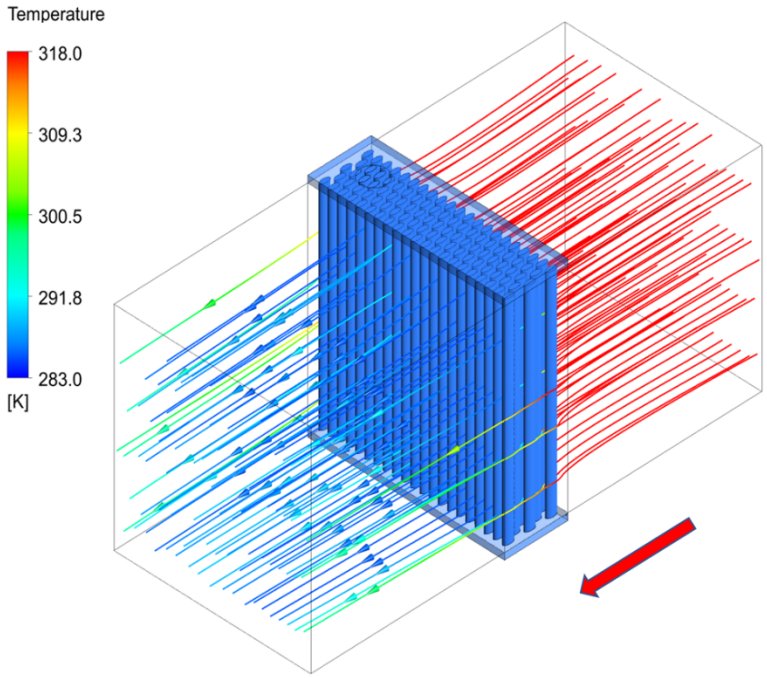

Figure 5: Airflow path from the reference case.

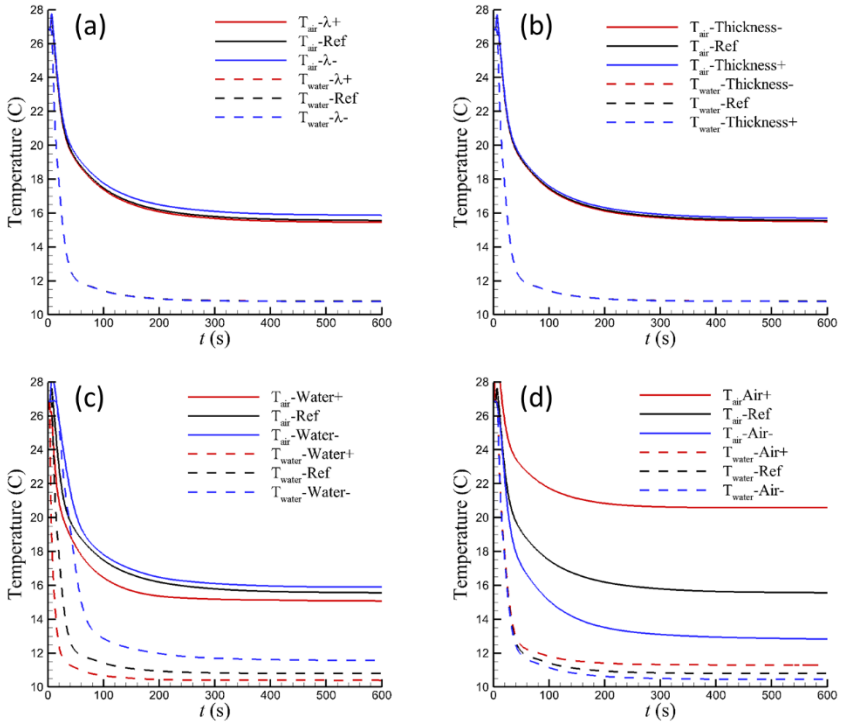

Figure 6: Temperatures at the air outlet and water outlet with changes of (a) thermal conductivity, (b) tube thickness (c) water flow velocity, and (d) air speed.

Table 2: Simulation results of the baseline cases

Case	Air inlet temperature (°C)	Water inlet temperature (°C)	Air outlet temperature (°C)	Water outlet temperature (°C)
Reference	45	10	15.559	10.792
λ−	45	10	15.867	10.784
λ+	45	10	15.450	10.795
Thickness−	45	10	15.493	10.794
Thickness+	45	10	15.691	10.788
Water−	45	10	15.913	11.564
Water+	45	10	15.074	10.393
Air−	45	10	12.822	10.445
Air+	45	10	20.588	11.298

Figure 6(a) shows the effect of tube thermal conductivity. Because the water's specific heat is much higher than that of air, the water outlet temperatures from case λ− and λ+ are very close to the reference case. The difference can be identified from the air outlets, which reveal that using a higher–thermal conductivity material to additively manufacture tubes would benefit the heat transfer performance of the heat exchanger because from 0.4 to 8 W/(m·K), the air outlet temperature changes significantly. However, the results also show that from 1.33 to 8 W/(m·K), the air outlet temperature does not significantly increase, indicating that tube thermal conductivity does not likely significantly enhance heat transfer performance of the polymer heat exchanger if the thermal conductivity is fair enough. Figure 6(b) demonstrates the tube wall thickness effect on the heat transfer performance. The thinner the tube, the better the performance of the heat exchanger, but the difference is insignificant, and 1 mm thickness is sufficiently thin to offer good performance. Figure 6(c) and 6(d) show the effects of water flow velocity and air velocity. Figure 6(c) shows that the fast water speed can help to cool the air (solid red line), and the water does not have enough time to absorb heat, thus resulting in the lowest water outlet temperature. Similarly, Figure 6(d) also reveals that high air velocity prevents water temperature increase but results in a high air temperature at the outlet. Therefore, the baseline simulation results suggest that the water and air velocities are high impact factors to influence the heat transfer performance of the heat exchanger. Moreover, the thermal conductivity and thickness of the tube in the baseline design are sufficient to offer good performance.

Because the performance of the heat exchanger can be controlled by changing the flow rate of both air and water, the air and water velocities can be adjusted to achieve the desired power. In this research, when the air velocity of the reference case was changed to 0.5 m/s, the simulation results indicate that the heat exchanger achieves 1 kW. From this baseline design, two more designs were developed as described to improve the heat exchanger performance. Simulations were conducted to reveal the heat transfer performance of the two improved heat exchanger designs. Because the baseline heat exchanger takes only a short time to reach a steady state, for designs Snake A and Snake B, only steady-state simulations were conducted to evaluate the power of the heat exhangers. Table 3 lists the simulation results for the baseline and improved designs. The results indicate that both Snake A and Snake B can improve the performance of heat exchanger in comparison to the baseline. Because of the additional fins, Snake A can achieve 1.113 kW. Moreover, when additional vertical fins are included, Snake B can achieve 1.126 kW. Both of the designs are feasible to fabricate via additive manufacturing, so the designs will be employed in future heat exchanger development and testing.

Table 3: Performance evaluations of the baseline, Snake A, and Snake B designs.

Case	Air outlet temperature (°C)	Air inlet temperature (°C)	Water outlet temperature (°C)	Water inlet temperature (°C)	Power (kW)
Baseline	27.400	45	11.900	10	1.000
Snake A	25.600	45	12.139	10	1.113
Snake B	24.888	45	12.147	10	1.126

5. CONCLUSIONS

A CFD model has been developed to model heat transfer performance of additively manufactured polymer heat exchangers. The model is implemented to model water to air heat exchangers in the present work. Parametric studies are conducted, which reveal water and air flow rates are key factors to influence the heat exchanger performance. In addition, building up with the baseline design, some fins are added to the heat exchanger to enhance the performance. The simulation results indicate that both "snakes" designs can improve the heat changers' performance by more than 10%.

REFERENCES

ANSYS (2017) *ANSYS FLUENT 17.2 Theory Guide*.
Ben-Ner, A. and Siemsen, E. (2017) 'Decentralization and Localization of Production', *California Management Review*, 59(2), pp. 5–23. doi: 10.1177/0008125617695284.
Bhargava, K. C., Thompson, B. and Malmstadt, N. (2014) 'Discrete elements for 3D microfluidics', *Proceedings of the National Academy of Sciences of the United States of America*, 111(42), pp. 15013–15018. doi: 10.1073/pnas.1414764111.
Cormier, Y. *et al.* (2013) 'Net shape fins for compact heat exchanger produced by cold spray', *Journal of Thermal Spray Technology*, 22(7), pp. 1210–1221. doi: 10.1007/s11666-013-9968-x.
Deylami, H. M. *et al.* (2013) 'Numerical investigation of using various electrode arrangements for amplifying the EHD enhanced heat transfer in a smooth channel', *Journal of Electrostatics*, 71(4), pp. 656–665. doi: 10.1016/j.elstat.2013.03.007.
Guo, H. *et al.* (2021) 'Highly Thermally Conductive 3D Printed Graphene Filled Polymer Composites for Scalable Thermal Management Applications', *ACS Nano*, 15(4), pp. 6917–6928. doi: 10.1021/acsnano.0c10768.
Kim, J. and Yoo, D. J. (2020) '3D printed compact heat exchangers with mathematically defined core structures', *Journal of Computational Design and Engineering*. Oxford University Press, 7(4), pp. 527–550. doi: 10.1093/jcde/qwaa032.
Maloney, K. J. *et al.* (2012) 'Multifunctional heat exchangers derived from three-dimensional micro-lattice structures', *International Journal of Heat and Mass Transfer*. Elsevier Ltd, 55(9–10), pp. 2486–2493. doi: 10.1016/j.ijheatmasstransfer.2012.01.011.
Ngo, T. L. *et al.* (2006) 'New printed circuit heat exchanger with S-shaped fins for hot water supplier', *Experimental Thermal and Fluid Science*, 30(8), pp. 811–819. doi: 10.1016/j.expthermflusci.2006.03.010.
Wang, G. *et al.* (2019) 'Experimental and numerical investigation of fractal-tree-like heat exchanger manufactured by 3D printing', *Chemical Engineering Science*, 195, pp. 250–261. doi: 10.1016/j.ces.2018.07.021.

ACKNOWLEDGEMENT

This work was sponsored by the U. S. Department of Energy's Building Technologies Office under Contract No. DE-AC05-00OR22725 with UT-Battelle, LLC. We would like to acknowledge Dr. Isaac Mahderekal the Technology Manager for the HVAC & Appliances for his support.